



**Post-assembly α -helix to β -sheet structural transformation
within SAF-p1/p2a peptide nanofibers**

Journal:	<i>Soft Matter</i>
Manuscript ID	SM-ART-08-2018-001754.R1
Article Type:	Paper
Date Submitted by the Author:	22-Oct-2018
Complete List of Authors:	Roberts, Evan; Georgia Institute of Technology, Chemical and Biomolecular Engineering Wong, Kong; Georgia Institute of Technology, Chemical and Biomolecular Engineering Lee, Elizabeth; Georgia Institute of Technology, Chemical and Biomolecular Engineering Le, Melina; Georgia Institute of Technology, Chemical and Biomolecular Engineering Patel, Dipam; Georgia Institute of Technology, Chemical and Biomolecular Engineering Paravastu, Anant K.; Georgia Institute of Technology, Chemical and Biomolecular Engineering



Journal Name

ARTICLE

Post-assembly α -helix to β -sheet structural transformation within SAF-p1/p2a peptide nanofibers

Evan K. Roberts, Kong M. Wong, Elizabeth J. Lee, Melina M. Le, Dipam M. Patel, and Anant K. Paravastu*

Received 00th January 20xx,
Accepted 00th January 20xx

DOI: 10.1039/x0xx00000x

www.rsc.org/

We report an unanticipated helix-to-sheet structural transformation within an assembly of SAF-p1 and SAF-p2a designer peptides. Solid-state NMR spectroscopic data support the assembled structure that was targeted by rational peptide design: an α -helical coiled-coil co-assembly of both peptides. Subsequent to assembly, however, the system converts to a β -sheet structure that continues to exhibit nearest-neighbor interactions between the two peptide components. The structural transition occurs at pH 7.4 and exhibits strongly temperature-dependent kinetics between room temperature (weeks) and 40 °C (minutes). We further observed evidence of reversibility on the timescale of months at 4 °C. The structural conversion from the anticipated structure to an unexpected structure highlights an important aspect to the challenge of designing peptide assemblies. Furthermore, the conformational switching mechanism mediated by a prerequisite α -helical nanostructure represents a previously unknown route for β -sheet designer peptide assembly.

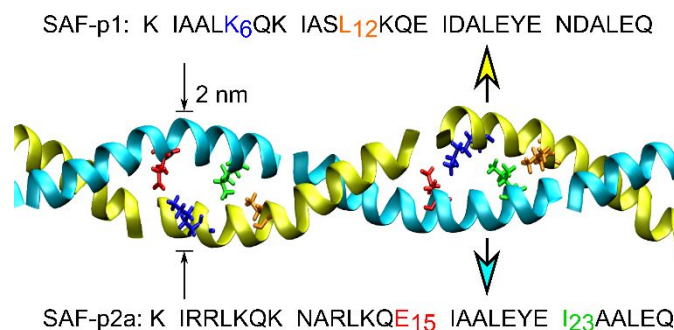


Fig. 1 The SAF-p1/p2a binary co-assembling peptide system, represented as an α -helical coiled-coil molecular model and as sequences of single-letter amino acid symbols. The presented molecular model is an all-atom model of the SAF-p1/p2a protofilament oriented such that the nanofiber axis is horizontal. A typical nanofiber is tens of nanometers in diameter, consistent with lateral association of many protofilaments. The complementary peptides SAF-p1 and SAF-p2a are drawn as yellow and light blue ribbons, respectively, with arrows of the same colors pointing to their amino acid sequences. The amino acids K6 and L12 of SAF-p1 and E15 and I23 of SAF-p2a were uniformly ¹³C-labeled for our NMR experiments, and are shown in blue, orange, red, and green, (respectively) using ball-and-stick representations in the molecular model and colored lettering in the amino acid sequences.

Introduction

Department of Chemical and Biomolecular Engineering, Georgia Institute of Technology, Atlanta, GA 30332, USA. *email: anant.paravastu@chbe.gatech.edu
Electronic Supplementary Information (ESI) available: [details of any supplementary information available should be included here]. See DOI: 10.1039/x0xx00000x

The SAF-p1 and SAF-p2a peptides are a binary peptide system in the “Self-Assembling Fiber” (SAF) family of complementary peptides, which were each rationally designed to adopt α -helical conformations and co-assemble upon mixing to form nanofibers comprised of structural subunits that follow the coiled-coil scheme for intermolecular organization.^{1,2} The design strategy to achieve desired post-assembly molecular arrangements and

material properties for each SAF system was implemented at the level of primary structure and generally follows the heptad repeat pattern $(hxxhcx)_n$, where n is 4 for most SAF sequences.³ The symbols h , c , and x represent positions occupied by amino acids with hydrophobic, charged, or non-hydrophobic sidechains, respectively—of these, the amino acids located at h and c positions are critical for mediating coiled-coil assembly because their sidechains repeat across the intermolecular interface formed when α -helical peptides dimerize in water.^{4–12} For SAF systems, amino acids at h and c positions were chosen to disfavor self-assembly of individual peptides and encourage complementary peptides to co-assemble into “sticky-ended” heterodimers, which further assemble longitudinally into extended coiled coils.

The primary structures of SAF-p1 and SAF-p2a are shown in Fig. 1 along with the anticipated SAF-p1/p2a protofilament structure (representative of a single extended coiled coil). Experimental evidence for the efficacy of the SAF peptide design includes measurements of secondary structure through techniques such as circular dichroism (CD), nanoscale measurements of assembly dimensions and morphologies, and demonstrated control of assembly characteristics through variations in peptide primary structure.^{1–3,13–15} Sharp *et al.* reported a structural model of the SAF-p1/p2a α -helical nanofiber based on transmission electron cryomicroscopy (cryo-TEM).¹⁶ In this model, protofilaments such as that depicted in Fig. 1 associate laterally in a hexagonally packed configuration to form nanofibers with widths previously determined to be on the order of 50–90 nm.¹³ However, direct experimental detection of the inter-peptide sidechain interactions predicted by rational design has not been previously reported.

We performed solid-state nuclear magnetic resonance (NMR) spectroscopy on samples that were isotopically labeled with ¹³C at every C-site within K6 and L12 of the SAF-p1 peptide and within E15 and I23 of the SAF-p2a peptide. This labeling scheme was designed to test the anticipated intermolecular interactions of residues at complementary h and c positions within the α -helical coiled-coil protofilament structure (Fig. 1). With this structure, we would expect solid-state NMR spectra to show signatures (peak positions) indicative of α -helical secondary structure as well as close proximity between pairs of ¹³C-labeled hydrophobic (SAF-p1 L12, SAF-p2a I23) and oppositely charged (SAF-p1 K6, SAF-p2a E15) amino acids. We present evidence that the initial SAF-p1/p2a assembled structure is indeed consistent with an α -helical coiled coil featuring the anticipated inter-residue proximities. However, the spectral observables attributable to a coiled coil were reliably obtained only when sample preparation and experimental conditions were specifically chosen to stabilize this structure. We subsequently present NMR evidence and supporting CD data that demonstrate a near-quantitative solid-state structural transformation to a β -sheet assembly, with kinetics that depend on sample temperature and are at least partially reversible.

Methods

Preparation of SAF-p1/p2a Nanofibers

Unlabeled SAF-p1 and SAF-p2a peptides were purchased as trifluoroacetate salts from CPC Scientific, Inc. (Sunnyvale, CA). Analysis by the supplier determined molecular weights of 3188.6 g/mol and 3337.9 g/mol for SAF-p1 and SAF-p2a, respectively, by electrospray ionization-assisted mass spectrometry and 92–93% sample purity by reverse-phase high performance liquid chromatography. Labeled peptides (used for enhanced-sensitivity solid-state NMR analysis) were similarly produced by CPC Scientific, Inc. using uniformly ¹³C-¹⁵N labeled amino acids with Fmoc (fluorenylmethyloxycarbonyl) protecting groups supplied from our inventory (sourced from Cambridge Isotope Laboratories, Inc.), which were incorporated at the sequence positions indicated in Fig. 1 during Fmoc-based solid-phase peptide synthesis.¹⁷

Direct centrifugation method for preparation of NMR samples. The method described by Bromley *et al.* was followed for SAF-p1/p2a nanofiber assembly.¹⁸ We reduced sample temperature to 4 °C during the final 6 h of ¹³C-labeled nanofiber maturation for reasons described subsequently. Prior to assembly, SAF-p1 and SAF-p2a were dissolved into separate 30 mL volumes of 10 mM MOPS (3-morpholinopropanesulfonic acid) supplied at pH 7.4 (Alfa Aesar) to produce 200 μ M stock solutions of each peptide. Mixing these stock solutions gave 60 mL of assembly media at a concentration of 100 μ M in each peptide. The nanofibers were allowed to mature for a total of 24 h for all samples. For samples with no isotopic labeling, the full 24 h assembly period elapsed at room temperature (22 °C). ¹³C-labeled nanofibers were incubated at 22 °C for the first 18 h and then refrigerated at 4 °C for the remaining 6 h of assembly to minimize structural heterogeneity in the sample from progression of the helix-to-sheet structural transition at room temperature, which would complicate the interpretation of NMR results. Nanofibers were first pelleted from assembly media in 13.2 mL Ultra-Clear® tubes via ultracentrifugation at 280,000 $\times g$ and 4 °C for 35 min using a Beckman Optima XPN-100 fitted with a SW-41 Ti swinging-bucket rotor. The pelleted nanofibers were then centrifuged using the same settings in a single tube equipped with a polycarbonate funnel insert and a 3.2 mm NMR rotor (Fig. S1). The NMR rotor was loaded to capacity with nanofibers during this centrifugation step, and immediately used for NMR experiments.

Lyophilization method for preparation of NMR samples. Stock peptide solutions were prepared and mixed together as described above. The assembly media vessels were allowed to incubate for 24 h at 22 °C prior to centrifugation at 17,000 $\times g$ for 45 min in a Beckman-Coulter Allegra X30-R tabletop centrifuge. After discarding the supernatant, centrifuge pellets of SAF-p1/p2a nanofibers were flash-frozen in liquid nitrogen, lyophilized (freeze-dried) overnight, and manually transferred to a Bruker 3.2 mm solid-state NMR rotor.

Preparation of nanofibers for CD spectroscopy. CD measurements were performed on an SAF-p1/p2a nanofiber sample initially prepared at a 100 μM concentration (in each peptide) at pH 7.4 in 10 mM MOPS buffer solutions. After allowing 24 h for peptide assembly into nanofibers, solutions were diluted three-fold using 10 mM MOPS buffer to achieve a concentration of 33 μM in each peptide immediately prior to measurement. Dilution was necessary to bring the far-UV (< 210 nm) peptide absorbance within the operational limits of the CD instrument.

Transmission Electron Microscopy (TEM)

SAF-p1/p2a nanofibers were deposited from assembly media onto 400-mesh lacey carbon-coated Cu electron microscopy grids (Ted Pella, Inc.) and stained with 1 wt% uranyl acetate. TEM micrographs were collected using a Hitachi HT-7700 electron microscope with an accelerating voltage of 80 keV.

Fourier transform analysis of TEM images (Fig. S2)

Selected SAF-p1/p2a nanofiber TEM images were initially rotated to align the peptide nanofiber axis with the horizontal axis. Regions of interest were cropped from the rotated images. Background correction to reduce noise was performed by applying a Gaussian blur through the Mathematica function GaussianFilter and subtracting the Gaussian blurred image data from the original cropped image data. Resulting background corrected images were Fourier transformed. Peak fits were also obtained by Gaussian peak fitting in Mathematica. Reported striation periodicities were averaged over the two peaks present in the Fourier transform and across the 5 selected images.

CD Spectroscopy

CD spectra were recorded using a ChirascanTM-plus spectropolarimeter (Applied Photophysics, Ltd.) fitted with a Peltier temperature controller. Spectra were recorded as ellipticities (millidegrees), baseline-corrected using 10 mM MOPS solutions, and converted to molar ellipticities ($\text{degrees cm}^2 \text{dmol}^{-1}$). Samples were held in a quartz cuvette with a 0.1 mm path length. Spectral bandwidth and step size were set to 1 nm and spectra were acquired in the 190–280 nm range at a sampling rate of 120 Hz. CD spectra were first collected for each sample at 20 $^\circ\text{C}$, and then the sample temperature was increased to either 37 $^\circ\text{C}$ or 40 $^\circ\text{C}$. For the sample studied at 37 $^\circ\text{C}$, spectra were initially collected every 2 min for 1 h and then every 30 min for 5 h. For the sample that was studied at 40 $^\circ\text{C}$, CD measurements were collected every 2 min for 26 min.

Solid-State NMR

One-dimensional (1D) ^{13}C NMR spectra were collected using the ^1H - ^{13}C cross polarization magic angle spinning (CPMAS) pulse sequence.^{19,20} Two-dimensional (2D) ^{13}C - ^{13}C NMR spectra were

collected using the finite-pulse radiofrequency-driven recoupling (fpRFDR) pulse pattern with a mixing time (τ_m) of < 2 ms to obtain precise chemical shift (δ_c) assignments, or else using the dipolar-assisted rotational resonance (DARR) pulse sequence with a τ_m of 50 ms or τ_m in the range of 500–1000 ms to map through-bond correlations within or detect spatial proximities between labeled residues, respectively.^{21–24}

A Bruker AVANCE III HD-700 spectrometer (field strength of 16.4 T) was used to collect all NMR spectra of ^{13}C -labeled α -helical SAF-p1/p2a nanofibers that were concentrated for analysis by ultracentrifugation at 4 $^\circ\text{C}$, as well as for 2D ^{13}C - ^{13}C DARR with a τ_m of 50 ms and 1D ^{13}C CPMAS experiments following the transition to β -sheets at 40 $^\circ\text{C}$. All solid-state NMR experiments on SAF-p1/p2a samples concentrated for analysis by lyophilization were performed at a field strength of 11.74 T and a temperature of 22 $^\circ\text{C}$ using a Bruker DRX-500 spectrometer. The DRX-500 was also used for all 1D ^{13}C CPMAS experiments on unlabeled SAF-p1/p2a as well as the 2D ^{13}C - ^{13}C DARR experiment with $\tau_m = 500$ ms on the ^{13}C -labeled β -sheet SAF-p1/p2a sample that was concentrated by ultracentrifugation following initial assembly and heated to 40 $^\circ\text{C}$ to trigger the helix-to-sheet transition. Bruker temperature control hardware was used to set and maintain sample temperature for all NMR experiments. Spectrometer calibrations were performed using adamantane and/or polycrystalline glycine, and all reported chemical shifts are referenced to DSS (4,4-dimethyl-4-silapentane-1-sulfonic acid).

All experiments on both spectrometers were performed using E-free 3.2 mm HCN triple-resonance probes.²⁵ A 15.4 kHz MAS speed was used for all high-field NMR experiments. On the DRX-500, MAS speeds were either 22 kHz (2D fpRFDR and 1D ^1H - ^{13}C CPMAS) or 10 kHz (2D DARR) for the lyophilized sample, 22 kHz (2D fpRFDR and 1D CPMAS) or 11 kHz (2D DARR) for the rehydrated sample, and 11 kHz for all other experiments. Rehydration of the lyophilized SAF-p1/p2a nanofibers was performed using ~ 1 μL ultra-pure water per mg sample.

Molecular Modelling

All-atom molecular models were built using NAMD molecular dynamics and CCBUILDER 2.0 software.^{26,27} Initial models were created with CCBUILDER 2.0 to fit a heterodimer coiled-coil structure with a radius of assembly (r) of 5.1 \AA , pitch (P) of 2260 \AA , interface angle ($\phi\text{C}\alpha$) of 0° , and z-shift of 22.0 \AA . The SAF-p1/p2a coiled-coil dimer was manipulated and repeated along the coiled-coil axis using Mathematica to produce a 10-unit (5 SAF-p1 and 5 SAF-p2a) peptide nanofiber. Artificial dihedral angle constraints were placed. Using NAMD molecular dynamics software, the structure was energy minimized for 5 ns in a vacuum. The temperature was increased from 0 K to 300 K in 10 K increments with 10 ps simulation time per step in a vacuum. Reported distances were calculated using coordinates from the inner four peptides (two of each peptide sequence) and averaged over the last 5 frames (5 ps) of the three lowest energy

simulations. By using the inner four peptides, end effects from unpaired peptide segments were minimized. Visualization of the SAF peptide nanofiber was done with VMD (Visual Molecular Dynamics) software.²⁸

Results

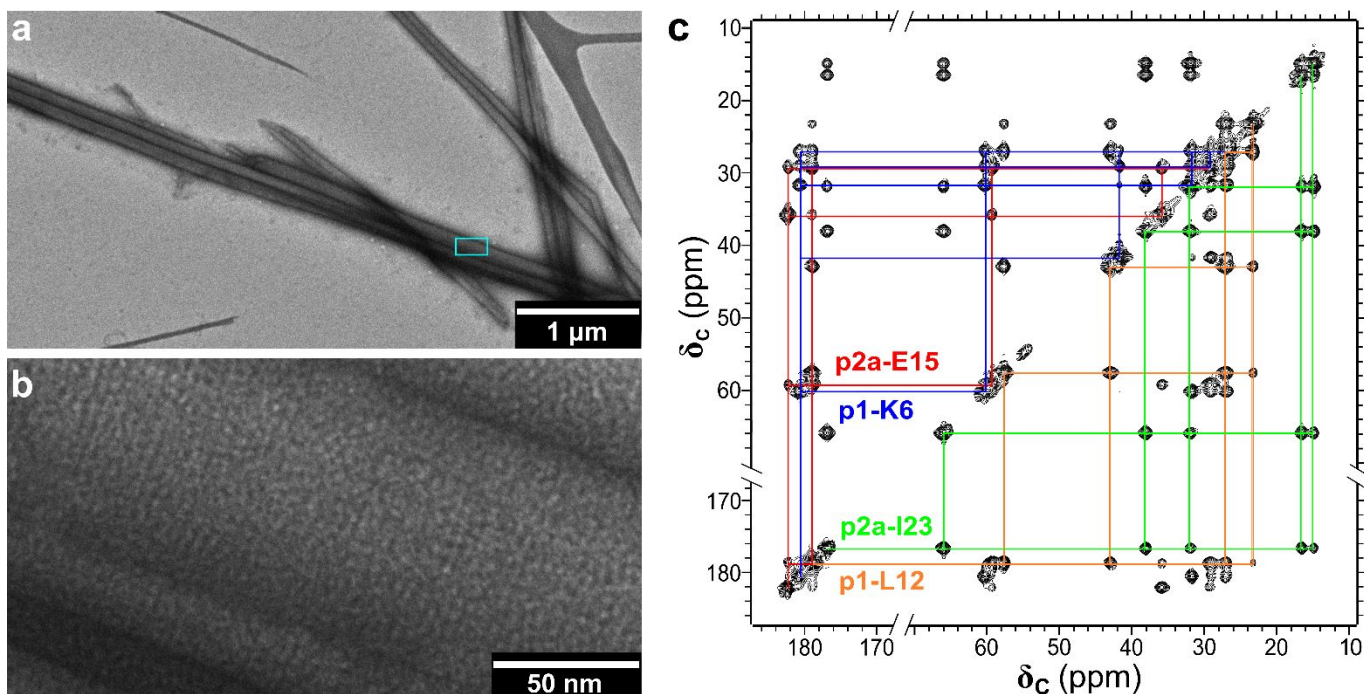
Initial SAF-p1/p2a assembly produces highly ordered α -helical nanofibers

Fig. 2 shows experimental evidence that SAF-p1/p2a assembles into α -helical nanofibers, as was reported previously.³ The nanofibers, imaged using negative-stain TEM, exhibited dimensions and morphologies that are consistent with previous measurements (Fig. 2a).^{3,13} The presence of α -helices within the nanofiber structure is supported by a characteristic light-to-dark surface striation pattern that repeats along the fiber axis (Fig. 2b).^{3,13,16} Fourier Transform analysis of fiber TEM images (Fig. S2) returned a striation periodicity of 4.5 ± 0.1 nm. We consider this measured striation periodicity to be reasonable but slightly larger than predicted and previously reported values. Theoretical estimates of the striation periodicity are 4.4 ± 0.2 nm and 4.14 nm, based on our modeling of the SAF-p1/p2a protofilament (Fig. 1) and the calculated length of an ideal 28-residue α -helix, respectively.²⁹ Previously measured values are 4.2 ± 0.1 and 4.18 nm, measured by TEM and cryo-TEM, respectively, with the additional use of positive staining and internal standards for length.^{3,16} The solid-state NMR spectrum in Fig. 2c, collected on an ultracentrifuge pellet of assembled SAF-p1/p2a nanofibers, exhibits α -helical spectral characteristics.³⁰⁻³² The frequency range plotted in Fig. 2c was chosen to more clearly show the signals of interest; the full spectrum is shown in Fig. S3. This spectrum was collected using the 2D ^{13}C - ^{13}C dipolar-assisted rotational resonance (DARR) NMR technique (see Methods).²³ The mixing

time employed for ^{13}C - ^{13}C dipolar recoupling ($\tau_m = 50$ ms) produces off-diagonal peaks (crosspeaks) corresponding to all pairs of ^{13}C -labeled sites

that are within the same amino acid.^{23,24} In 2D DARR spectra, crosspeak patterns are approximately symmetric about the diagonal (line where frequencies are the same on both axes). To illustrate correspondence between NMR peaks and ^{13}C -labeled sites (spectral assignments), horizontal and vertical colored lines are drawn to connect diagonal peaks and crosspeaks corresponding to NMR signals from atoms within the same amino acid. Table S1 comprehensively reports the spectral assignments through the NMR frequency and peak width of every ^{13}C -labeled site. These assignments were determined based on crosspeak patterns that are unique to each amino acid.^{24,30} Peptide secondary structure was assessed using the ^{13}C NMR frequencies (δ_c) of ^{13}C -labeled backbone carbonyl (CO), α -carbon (C_α) and β -carbon (C_β) sites; secondary chemical shifts reported by Table 1 are frequencies relative to those measured for equivalent sites within random-coil model peptides ($\Delta\delta_c = \delta_{c,\text{sample}} - \delta_{c,\text{random coil}}$).^{24,31,33} For α -helical secondary structure, $\Delta\delta_c$ is characteristically positive ($> \sim 1.0$ ppm) for CO and C_α signals and below or near zero for C_β signals.³⁰⁻³⁴

The molecular structure of assembled α -helical SAF-p1/p2a peptides is highly ordered and uniform throughout the sample. The ^{13}C NMR peak widths in Fig. 2c are 0.6 ± 0.2 ppm full width at half maximum (FWHM), similar to those observed in ^{13}C NMR spectra of protein crystals.³⁵ A single NMR peak is observed for each ^{13}C -labeled site, indicating a single molecular conformation for each peptide. These results are consistent with the cryo-TEM study of Sharp *et al.*, in which the structural order was sufficient to produce a molecular structural model of hexagonally-packed SAF-p1/p2a coiled-coil protofilaments.¹⁶



4 | J. Name., 2012, 00, 1-3

This journal is © The Royal Society of Chemistry 20xx

Fig. 2 TEM images and 2D DARR spectrum of initial coiled-coil nanofiber assembly. (a) Negative-stain TEM image of SAF-p1/p2a nanofibers at low magnification. (b) Higher-magnification TEM image of the region defined by the blue box in Panel a. (c) 2D ^{13}C - ^{13}C DARR spectrum collected on SAF-p1/p2a nanofibers at 4 °C with $\tau_m = 50$ ms. Sets of colored horizontal and vertical lines are drawn between diagonal peaks and crosspeaks connecting all ^{13}C NMR signals from each labeled residue; representative colors for these residues are indicated on the spectrum. These patterns indicate spectral assignments for ^{13}C -labeled residues.⁵

Despite the high degree of structural order, we did not observe the α -helical SAF-p1/p2a assembly to be stable under commonly employed experimental conditions. Solid-state NMR experiments on peptide assemblies are often conducted near room temperature on samples concentrated by lyophilization,³⁶ but we found that these experimental conditions promote instability of SAF-p1/p2a α -helical assemblies. For this reason, we avoided lyophilization during sample preparation by centrifuging freshly matured SAF-p1/p2a nanofibers directly into the solid-state NMR sample holder (rotor) and maintained a sample temperature of 4 °C to obtain the NMR spectrum in Fig. 2c (see Methods).³⁷ A photograph of the polycarbonate funnel used to transfer SAF-p1/p2a nanofibers into the NMR rotor during centrifugation is shown in Fig. S1. The consequences of increased sample temperature and lyophilization are presented subsequently.

Table 1 ^{13}C NMR chemical shifts (δ_{C}) and secondary ^{13}C chemical shifts ($\Delta\delta_{\text{C}}$) of near-backbone labeled sites in SAF-p1/p2a α -helical nanofibers.^{5,6} Chemical shift assignments are derived from the 2D DARR spectrum in Fig. 2c.

	δ_{C} (ppm)			$\Delta\delta_{\text{C}}$ (ppm)		
	CO	C_{α}	C_{β}	CO	C_{α}	C_{β}
SAF p1-K6	180.5	60.3	31.9	3.9	4.1	-1.2
SAF p1-L12	178.8	57.7	43.1	1.2	2.6	0.7
SAF p2a-E15	178.9	59.4	29.5	2.3	2.8	-0.4
SAF p2a-I23	176.8	66.0	38.3	0.4	4.9	-0.5

Increasing sample temperature to 40°C induces a rapid, near-quantitative structural transition to β -sheets

A change in the SAF-p1/p2a molecular structure was observed when the temperature of the sample used to collect the NMR spectrum in Fig. 2c was raised above 4 °C. This structural transition was evident in the ^{13}C NMR spectra, as shown in Fig. 3 for a sample temperature increase to 40 °C. Fig. 3a compares the 1D (single frequency axis) ^{13}C NMR spectrum obtained from the α -helical nanofibers at 4 °C to that taken once the ^{13}C NMR spectrum stabilized after ~ 25 min at 40 °C (see Methods). The assignment of β -strand secondary structure is based on secondary chemical shift values ($\Delta\delta_{\text{C}}$, see Table 2) obtained from the 2D ^{13}C - ^{13}C DARR spectrum ($\tau_{\text{m}} = 50$ ms) in Fig. 3b, which was measured after the structural transition at 40 °C. Negative $\Delta\delta_{\text{C}}$ values (< -0.5 ppm) for CO and C_{α} concurrent with positive $\Delta\delta_{\text{C}}$ values (> 0.5 ppm) for C_{β} are associated with β -strand secondary structure.^{30-32,34} Since β -strands are unstable in isolation, they are expected to organize into β -sheets—we therefore refer to the structural transition as a “helix-to-sheet” transition.³⁸ Table S2 reports all the ^{13}C NMR peak

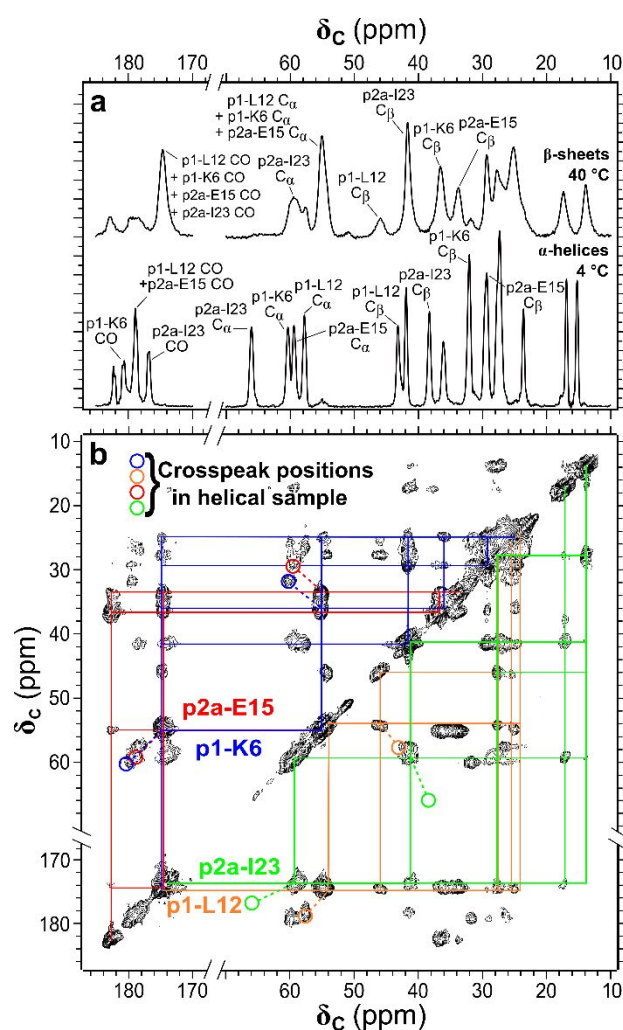


Fig. 3 NMR spectra showing the effect of SAF-p1/p2a β -sheet formation. (a) 1D ^{13}C NMR spectra collected on assembled SAF-p1/p2a before (below) and after (above) the structural transition induced by increasing the sample temperature from 4 °C to 40 °C. To illustrate changes in peak positions, the locations of CO, C_{α} , and C_{β} NMR peaks are indicated for each ^{13}C -labeled amino acid. (b) 2D ^{13}C - ^{13}C DARR spectrum ($\tau_{\text{m}} = 50$ ms) collected after heating SAF-p1/p2a nanofibers to 40 °C. Colored circles and dashed lines show the positions of structure-sensitive crosspeaks following initial assembly at 4 °C (Fig. 2c) and their changes in position upon heating to 40 °C, respectively.⁵

positions and widths measured after the structural transition. It is notable that the helix-to-sheet transition is not accompanied by loss of NMR signal from any ^{13}C -labeled site (beyond a 10% measurement error), indicating that both SAF-p1 and SAF-p2a undergo the transition without disassembly or dissolution. It is also notable that the β -sheet assembly is structurally ordered, but less structurally ordered than the α -helical assembly: the β -sheet assembly exhibits NMR peak widths of 1.3 ± 0.6 ppm. Peak widths for amyloid fibrils, which are also β -sheet assemblies, can vary between 0.25 and 2 ppm depending on structural homogeneity.³⁹⁻⁴² Finally, we point out that detectable signal persists at ^{13}C NMR frequencies that are characteristic of α -helical structure (particularly in the portion of the CO region spanning 176-180 ppm) following the structural transition—this evidence of a surviving α -helical structural population (roughly 10% of the sample) compels us to refer to the helix-to-sheet transition as “near-quantitative” rather than “quantitative”. The 2D DARR spectra from Figs. 2c and 3b are overlaid in Fig. S4 for comparison.

TEM images taken following the helix-to-sheet transition show a conversion from large, striated fibers to more fragmented fibrils. Samples of assembled SAF-p1/p2a were heated at 37 °C for 6 h, revealing a structural change towards globular peptide assemblies and “worm-like” fibrils from α -helical fibers in Figs. 4a and S5a-b). These globular aggregates (Fig. S5a) and fibrils are similar to structures seen during amyloid-like assembly processes.⁴³ Unlike the pristine α -helical nanofiber samples, the worm-like fibrils do not exhibit striations perpendicular to the fiber axis (Fig.4b). The loss of surface striations is consistent with the change in structure observed in the NMR data. After heating, the β -sheet samples shown in Fig. 4a-b were refrigerated overnight (18 h) at 4 °C and imaged subsequently (Fig. 4c-d). Surprisingly, refrigerated samples form short, straight fibrils and are absent of globular

Table 2 ^{13}C NMR chemical shifts (δ_{C}) and secondary ^{13}C chemical shifts ($\Delta\delta_{\text{C}}$) measured following the helix-to-sheet transition.⁵⁶ Chemical shift assignments are derived from the 2D DARR spectrum in Fig. 3b.

	δ_{C} (ppm)			$\Delta\delta_{\text{C}}$ (ppm)		
	CO	C_{α}	C_{β}	CO	C_{α}	C_{β}
SAF p1-K6	174.8	55.1	36.0	-1.8	-1.1	2.9
SAF p1-L12	174.8	54.0	46.0	-2.8	-1.1	3.6
SAF p2a-E15	174.4	55.0	33.5	-2.2	-1.6	3.6
SAF p2a-I23	173.7	59.3	41.3	-2.7	-1.8	2.5

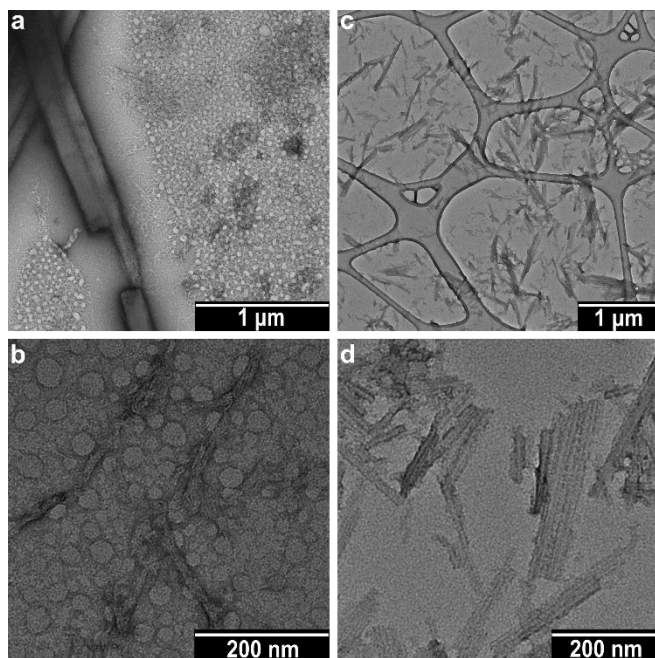


Fig. 4 Negative-stain TEM images of SAF p1/p2a following the helix-to-sheet structural transition. (a-b) Low and high magnification images of co-assembled α -helical nanofibers heated at 37 °C for 6 h. (c-d) Low and high magnification images of the samples from Panels a-b taken after refrigeration at 4 °C for 18 h.

assemblies. Close examination of the fibril structure reveals striations along the fiber axis (Figs. 4d and S5c). Refrigeration of the samples may allow globular aggregates and “worm-like” fibrils to reorganize into more ordered, straight fibrils similar to structural reorganization observed in amyloid-like fibers.⁴³

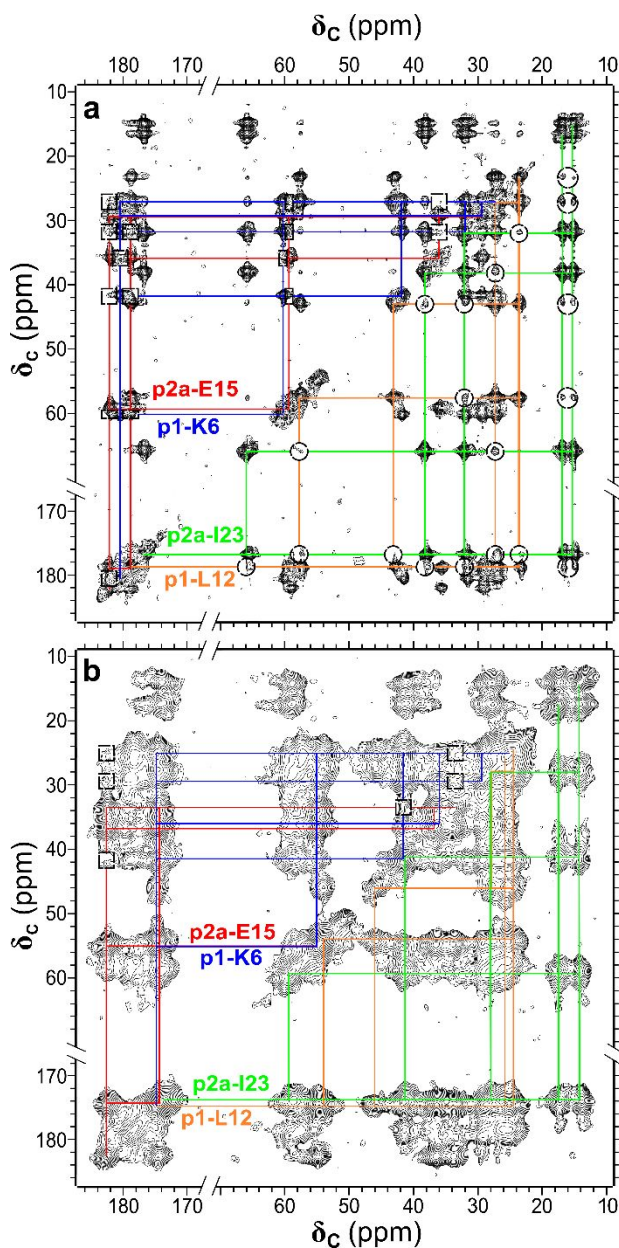


Fig. 5 Evidence of co-assembly before and after the helix-to-sheet structural transition. (a) 2D ^{13}C - ^{13}C DARR spectrum collected at 4 °C with $\tau_m = 1000$ ms on the isotopically labeled α -helical SAF-p1/p2a nanofiber sample. Colored lines indicate the same spectral assignments as in Fig. 2c.⁵ Circled or boxed crosspeaks result from inter-residue ^{13}C - ^{13}C dipolar couplings between SAF-p1 L12 and SAF-p2a I23 or between SAF-p1 K6 and SAF-p2a E15, respectively. (b) 2D ^{13}C - ^{13}C DARR spectrum collected with $\tau_m = 500$ ms on the β -sheet SAF-p1/p2a sample from Fig. 3; colored lines indicate the same spectral assignments as in Fig. 3b.⁵ Crosspeaks above the diagonal that result from inter-residue dipolar couplings between SAF-p1 K6 and SAF-p2a E15 are boxed.

Helix-to-sheet structural transition does not segregate the two peptides

By collecting 2D DARR spectra at mixing times long enough to observe inter-residue proximities (above 500 ms),^{24,44} we observed that the helix-to-sheet structural transition occurs without molecular-level separation of the SAF-p1 and SAF-p2a

peptides. Molecular-level association of the two peptide components was anticipated by design for the α -helical assembly and experimentally detected in the 2D DARR spectrum collected at 4 °C with $\tau_m = 1000$ ms (Fig. 5a), which exhibits NMR crosspeaks between SAF-p1 L12 and SAF-p2a I23 (circled below the diagonal) as well as between SAF-p1 K6 and SAF-p2a E15 (boxed above the diagonal). The observation of crosspeaks corresponding to pairs of ^{13}C atoms on different residues indicates an inter-residue proximity of 0.6 nm or less,⁴⁵ and the particular sets of inter-residue crosspeaks observed here also indicate co-assembly of complementary peptides. Inter-residue crosspeaks in the 2D DARR spectrum are additionally shown in Fig. S6, which compares selected slices (1D cross-sections) taken from the spectrum in Fig. 5a. The 2D DARR spectrum depicted in Fig. 5b was measured at 40 °C with $\tau_m = 500$ ms after the helix-to-sheet structural transition. In this spectrum, we detected crosspeaks between SAF-p1 K6 and

SAF-p2a E15 (dashed boxes above the diagonal, 1D slices shown in Fig. S7), but not between SAF-p1 L12 and SAF-p2a I23. The observation of crosspeaks between SAF-p1 K6 and SAF-p2a E15 in both Fig. 5a and Fig. 5b indicates that, despite a dramatic change in molecular conformation, the SAF-p1 and SAF-p2a peptides remain associated at the molecular level after the helix-to-sheet structural transition.

Helix-to-sheet structural transition exhibits temperature-dependent kinetics and reversibility

To probe temperature-dependent kinetics of the helix-to-sheet structural transition, we performed time-dependent measurements of the natural abundance (no isotopic labeling) ^{13}C NMR spectrum on assembled SAF-p1/p2a following changes in sample temperature. The 1D ^{13}C NMR spectra shown in Fig. 6 include approximately equal contributions from the 1% of

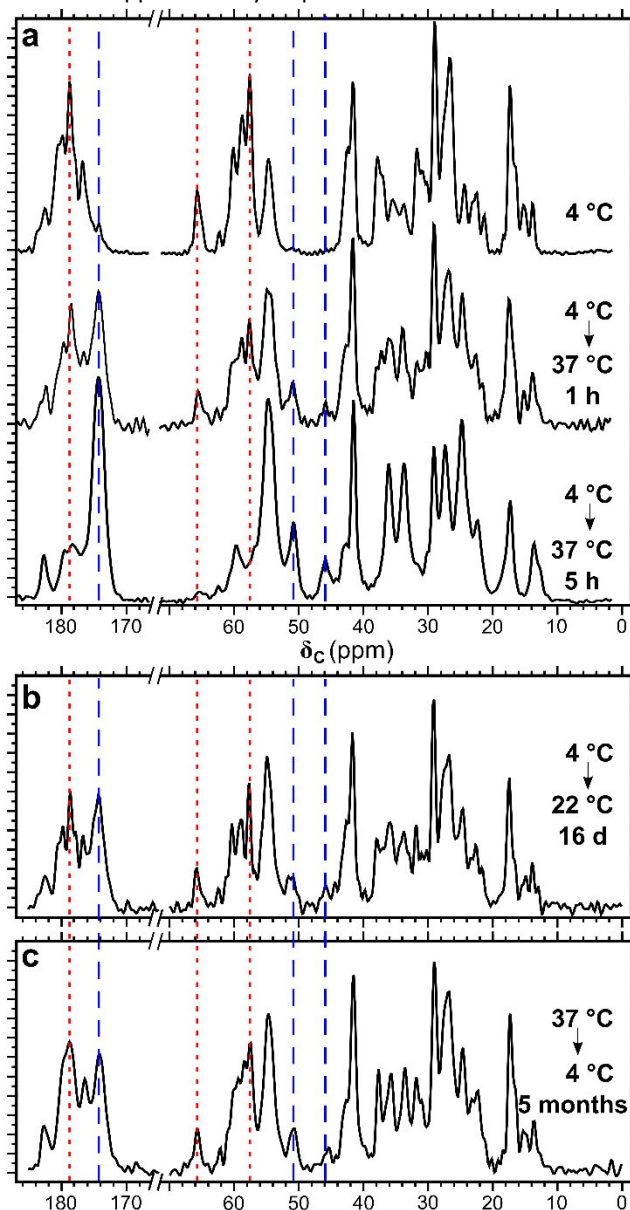


Fig. 6 ^{13}C NMR spectra exhibiting kinetic behavior and reversibility of the helix-to-sheet transition in SAF-p1/p2a samples with no isotopic labeling. Natural abundance ^{13}C NMR spectra of (a) freshly centrifuged SAF-p1/p2a nanofiber pellet at 4 °C and after heating to 37 °C, (b) nanofibers centrifuged at 4 °C and left at room temperature for 16 days, and (c) the post-transition sample (Panel a, bottom) after 5 months of refrigeration at 4 °C. Red dotted and blue dashed vertical lines indicate peaks assigned to the α -helical and β -sheet structures, respectively.

naturally abundant ^{13}C atoms distributed uniformly amongst all C sites in each peptide. We restrict our analysis of natural-abundance ^{13}C NMR data to 1D NMR spectra because detectable 2D NMR crosspeaks are not expected without isotopic enrichment.²⁴ Nevertheless, we were able to identify and assign spectrally isolated NMR peaks in the 1D spectra that are exclusively associated with the α -helical or β -sheet structures, based on known chemical shift ranges for different C sites and information from the isotopically labeled samples (Figs. 2c and 3). Peaks assigned solely to the α -helical and β -strand structure are indicated in Fig. 6 with red and blue vertical dashed lines, respectively. The red vertical dashed lines at 178.4, 65.8, and 57.7 ppm correspond to NMR signals from α -helical backbone CO atoms (multiple amino acids), C_α atoms of Ile residues, and C_α atoms of Leu residues, respectively. The blue vertical dashed lines at 174.2, 51.0, and 46.0 ppm indicate NMR signals from β -strand backbone CO atoms (multiple amino acids), C_α atoms of Ala residues, and C_β atoms of Leu residues, respectively. Fig. 6a shows the natural abundance ^{13}C NMR spectrum of an α -helical SAF-p1/p2a assembly measured at 4 °C compared to spectra collected 1 h and 5 h after the sample temperature was increased to 37 °C. Additional ^{13}C NMR spectra collected subsequently at 37 °C (not shown) indicated no further structural change. Based on the intensities of the peaks marked by vertical dashed lines, we estimate that the sample initially contained a small but detectable fraction of β -strands (probably formed after initial coiled-coil peptide assembly and prior to centrifugation at 22 °C), approximately equal fractions of α -helices and β -strands after 1 h at 37 °C, and 90% β -strands after 5 h at 37 °C. The spectrum in Fig. 6b was collected on a different sample of α -helical SAF-p1/p2a nanofibers 16 days after the sample temperature was increased from 4 °C to 22 °C. The approximately equal contributions to NMR signals from α -helices and β -strands in this spectrum indicate that the structural transition occurs much more slowly at 22 °C than at 37 °C.

The spectrum in Fig. 6c indicates that helix-to-sheet structural transition is reversible at 4 °C, at least in terms of secondary structure. This spectrum exhibits approximately equal amounts of α -helical and β -strand NMR signals, but was collected on a sample that had been mostly composed of β -strands (the same sample used for the spectra in Fig. 6a) after its temperature was returned to 4 °C for 5 months. We restrict our interpretation to secondary structure because chemical shift data alone do not report on intermolecular organization. Therefore, it is not presently apparent whether the helix-to-sheet structural transition is reversible in terms of supramolecular organization.

The spectra in Fig. 6 further motivate the interpretation that the helix-to-sheet structural transition involves the full lengths of the SAF-p1 and SAF-p2a peptide backbones. All of the signals marked with vertical dashed lines, including the peaks assigned to a single amino acid type (Ile, Leu, and Ala), correspond to multiple amino acids within both primary structures due to their distribution across both amino acid sequences (Fig. 1). NMR peak

widths of ~ 2 ppm (FWHM) are much narrower than the differences in site-specific values for δ_{C} observed before and after the helix-to-sheet structural transition (Tables 1 and 2), and do not change in width or position as the relative contributions of α -helices and β -strands change between spectra in Fig. 6a. We infer from these observations that the helix-to-sheet transition occurs with individual peptide molecules of both SAF-p1 and SAF-p2a changing secondary structure across their full backbone lengths without long-lived intermediate states in which secondary structure varies from either conformation across individual peptide molecules.

The CD spectra in Fig. 7 corroborate the occurrence of the helix-to-sheet transition and provide a basis for comparison to previous work. When measured immediately following assembly, CD spectra (black lines in Fig. 7a-b) are consistent with α -helical structure and previous reports, exhibiting characteristic minima for an α -helix that are redshifted from the typical values of 222 nm and 208 nm (presumably due to scattering of the incident light by large nanofibers in the sample).^{1,13,46} As reported previously for this and other SAF variants, there is a large change in the CD spectra when temperature is increased to near 40 °C.^{13,47} This change was previously interpreted in terms of molecular disassembly via thermal denaturation, which would not be consistent with the data in Figs. 3-6: the observed NMR intensities and spectral features indicate a transition from one ordered structure to another without molecular dissolution, while TEM indicates that the nanoscale dimensions of the β -sheet structure remain much larger than the molecular dimensions of component peptides despite changes in morphology relative to the α -helical structure. The kinetics of the structural transition are considerably slower than may have been previously understood.⁴⁷

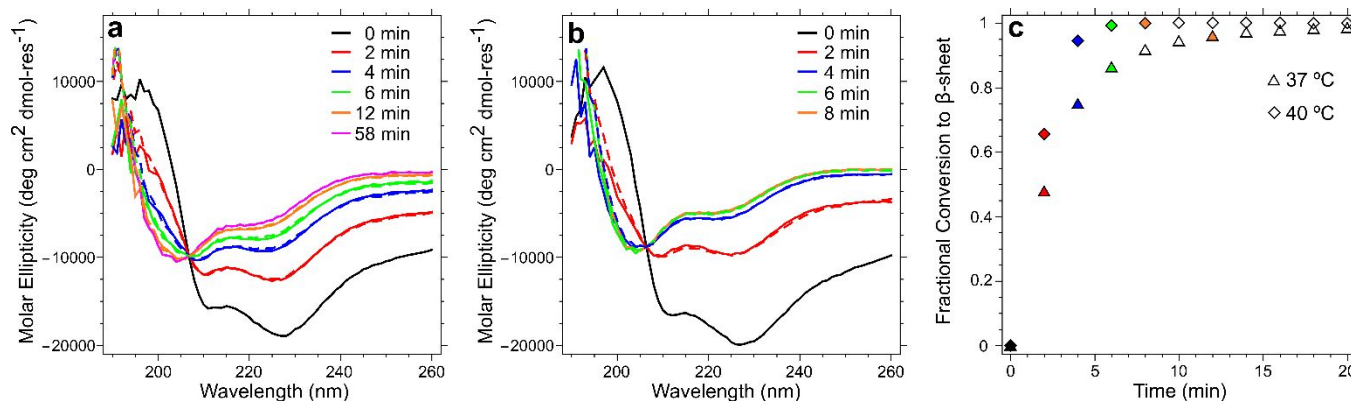


Fig. 7 Time-dependent CD spectra collected on SAF-p1/p2a coiled-coil nanofibers at (a) 37 °C and (b) 40 °C, showing the change in structure to β -sheets from an initially α -helical state (black curves, 0 min). The spectra collected at 58 min and 8 min for 37 °C and 40 °C data sets, respectively, are representative of the final β -sheet structure. For every CD spectrum collected during the transition, a dashed curve is drawn corresponding to a fractional weighted average of the α -helical and β -sheet spectra measured at each temperature. (c) Time dependence of fractional conversion to β -sheets measured at 37 °C (triangles) and 40 °C (diamonds). Colors of some symbols indicate correspondence to spectra shown in Panels a or b.

Consistent with the NMR-based observation that structural intermediates are not present in large populations, we found that the CD spectra collected at each temperature are well-represented by summation of the initial α -helical spectrum scaled by $1 - x$ and the final β -sheet spectrum scaled by x . The variable x represents fractional conversion from the α -helical to the β -sheet structure, and was evaluated for each CD spectrum by nonlinear regression. The dashed curves in Figs. 7a and b, which result from this analysis, show good agreement with the solid curves of the same color. The kinetic curves in Fig. 7c correspond to the best-fit values of x versus time at the indicated temperature. These time dependences are more accurate than those observed by NMR, since magic angle spinning and radio frequency excitations are known to induce temperature gradients across the sample.^{48,49}

Helix-to-sheet structural transition can also be induced by lyophilization and rehydration at room temperature

On a final experimental note, Figs. S7 and S8 show evidence for an alternative set of conditions for the helix-to-sheet structural transition. We observed this transition when SAF-p1/p2a nanofiber samples that were concentrated for NMR measurements by lyophilization were rehydrated with 1 μ L of water per mg of peptide at room temperature. Sample concentration by lyophilization instead of ultracentrifugation produced 2D NMR spectra that are consistent with α -helical structure (Figs. S8a and S9a), but with considerably broader NMR peaks (2-3 ppm FWHM) than the spectrum in Fig. 2c. Lyophilization-induced broadening is not unusual for peptide assemblies, and has been observed with amyloid fibrils—for those β -sheet aggregates, rehydration with \sim 1 μ L of water per mg of peptide is known to reverse lyophilization-induced line-broadening without affecting the molecular structure.^{39,50} Dissimilarly, when water was reintroduced to lyophilized α -helical SAF-p1/p2a nanofibers at 22 °C, we observed a rapid (several

hours) conversion of structure to β -sheets without sample heating (Fig. S8b). Furthermore, 2D DARR spectra and 1D slices in Figs. S9-S12 show that the same inter-residue proximities are detected before and after the helix-to-sheet transition as in Fig. 5, suggesting that lyophilization and rehydration induce a similar structural transformation as that induced by heating of ultracentrifuge pellets.

Discussion and conclusions

The present study demonstrates that the SAF-p1/p2a assembly is initially consistent with its design-targeted α -helical coiled-coil nanostructure, and then transitions to an unanticipated β -sheet structure at temperatures between 20 °C and 40 °C. NMR and CD spectra show that this transition exhibits temperature-dependent kinetics consistent with coexistence of only 2 structural states. TEM data indicate significant changes in nanoscale morphologies that accompany the structural transition. NMR data are not consistent with peptide dissolution or loss of ordered structure.

Peptide assemblies that undergo controllable solid-state structural transformations could have interesting material properties. The dramatic change in molecular conformation realized across highly ordered intermolecular arrangements is a basis for stimulus-responsive changes in nanoscale dimensions that could affect material behavior on a much larger scale. For example, since peptides and other small molecules have been shown to selectively bind to either α -helices or β -sheets, peptide structural transformation on a supramolecular scale could be a basis for selective encapsulation and controlled release.⁵¹⁻⁵⁶

Our observation of the helix-to-sheet transition highlights important aspects of the materials design challenge for peptide assemblies. In general, solid-state transformations could produce structures that are not solely determined by the solution-state assembly mechanism. We have previously reported that another peptide (RADA16-I) can undergo assembly in the solid-state, but the initial state in this case was a disordered precipitated

powder.^{57,58} It is significant that the SAF-p1/p2a system can produce β -sheet structure without an assembly mechanism resembling that of amyloid formation (addition of β -strands to β -sheets in solution) or otherwise requiring the dissolution of an initially α -helical assembly.^{46,47} While previous reports on designer peptides include some that can transition from α -helical to β -strand secondary structures, such transitions are reported to occur for α -helices in a soluble state, such that β -strand formation is considered a trigger for self-assembly rather than a post-assembly process.^{52,55,59-62}

Although we do not have complete knowledge of the SAF-p1/p2a β -sheet structure, its intermolecular configuration may differ from the cross- β amyloid structures (β -strands oriented perpendicular to the fibril axis) of other known β -sheet forming designer peptides.^{63,64} The reversible helix-to-sheet structural transformation reported here is reminiscent of early fiber diffraction work on α -keratin, a natural coiled-coil that rearranges into filaments of β -sheets (β -keratin) when stretched under steam and gradually recovers α -helical structure when tension and heat are removed.⁶⁵ The intermolecular alignments of α -keratin and β -keratin have since been shown to be similar to one another.⁶⁶ Analogously, the ability of thermally treated SAF-p1/p2a to recover its original α -helical secondary structure at low temperature suggests that intermolecular organization in the β -sheet may resemble that of the initial α -helical assembly. Furthermore, while most amyloid assemblies are composed exclusively of equivalent peptide molecules, the SAF-p1/p2a β -sheet includes two distinct peptides in close proximity—a property conserved from its initial coiled-coil configuration that exists in only a few designed β -sheet peptide systems.⁶⁷⁻⁶⁹ Because coiled-coil peptide assembly is well-studied and largely predictable from a structural design perspective,⁷⁰ a molecular-level understanding of the helix-to-sheet transition mechanism observed in SAF-p1/p2a could potentially unlock design strategies to deliberately access complex β -sheet arrangements of distinct peptide sequences via stimulus-activated transformation of co-assembled coiled-coils.

Conflicts of interest

There are no conflicts to declare.

Acknowledgements

This research was supported by funds from the National Science Foundation Grant DMR-105521 to A. K. P. The authors acknowledge the use of instruments in the NMR Center and Biopolymer Characterization Core at the Georgia Institute of Technology and the Robert P. Apkarian Integrated Microscopy Core at Emory University. We thank Benjamin C. Hudson for his assistance in performing CD measurements.

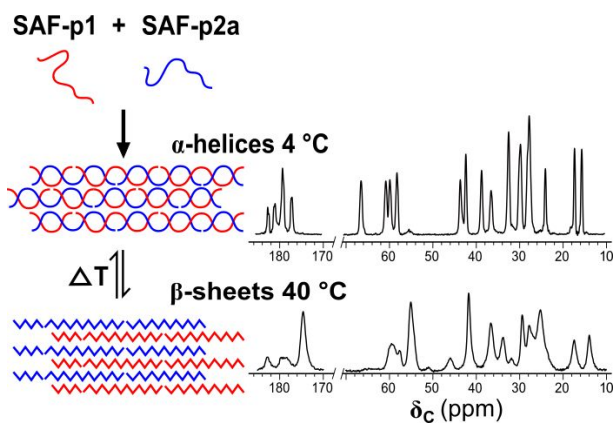
Notes and references

§ Although 2D DARR NMR spectra are approximately symmetric about the diagonal (line where δ_c is the same on both axes), all lines of a single color are drawn on a selected side of the diagonal to avoid clutter.

§§ Calculation of $\Delta\delta_c$ values was performed using random-coil chemical shifts from Wishart *et al.*³¹

1. M. J. Pandya, G. M. Spooner, M. Sunde, J. R. Thorpe, A. Rodger and D. N. Woolfson, *Biochemistry*, 2000, **39**, 8728-8734.
2. M. G. Ryadnov and D. N. Woolfson, *Nature Materials*, 2003, **2**, 329-332.
3. D. Papapostolou, A. M. Smith, E. D. Atkins, S. J. Oliver, M. G. Ryadnov, L. C. Serpell and D. N. Woolfson, *Proc. Natl. Acad. Sci. U. S. A.*, 2007, **104**, 10853-10858.
4. D. N. Woolfson, in *Fibrous Proteins: Coiled-Coils, Collagen and Elastomers*, eds. D. A. D. Parry and J. M. Squire, Elsevier, 2005, vol. 70, ch. 4, pp. 80-113.
5. A. N. Lupas and M. Gruber, in *Fibrous Proteins: Coiled-Coils, Collagen and Elastomers*, 2005, vol. 70, pp. 37-+.
6. B. Tripet, K. Wagschal, P. Lavigne, C. T. Mant and R. S. Hodges, *J. Mol. Biol.*, 2000, **300**, 377-402.
7. I. Drobnak, A. Ljubetic, H. Gradisar, T. Pisanski and R. Jerala, in *Protein-based Engineered Nanostructures*, eds. L. A. Cortajarena and T. Z. Grove, Springer, Switzerland, 2016, vol. 940, ch. 2, pp. 7-28.
8. Y. B. Yu, *Adv. Drug Del. Rev.*, 2002, **54**, 1113-1129.
9. J. R. Litowski and R. S. Hodges, *J. Biol. Chem.*, 2002, **277**, 37272-37279.
10. W. D. Kohn and R. S. Hodges, *Trends Biotechnol.*, 1998, **16**, 379-389.
11. E. H. Egelman, C. Xu, F. DiMaio, E. Magnotti, C. Modlin, X. Yu, E. Wright, D. Baker and V. P. Conticello, *Structure*, 2015, **23**, 280-289.
12. M. Goldstein, S. Rinne, A. K. Kiper, D. Ramirez, M. F. Netter, D. Bustos, B. Ortiz-Bonnin, W. Gonzalez and N. Decher, *Sci. Rep.*, 2016, **6**, 19492.
13. A. M. Smith, E. F. Banwell, W. R. Edwards, M. J. Pandya and D. N. Woolfson, *Adv. Funct. Mater.*, 2006, **16**, 1022-1030.
14. D. Papapostolou, E. H. C. Bromley, C. Bano and D. N. Woolfson, *J. Am. Chem. Soc.*, 2008, **130**, 5124-5130.
15. E. F. Banwell, E. S. Abelardo, D. J. Adams, M. A. Birchall, A. Corrigan, A. M. Donald, M. Kirkland, L. C. Serpell, M. F. Butler and D. N. Woolfson, *Nature Materials*, 2009, **8**, 596-600.
16. T. H. Sharp, M. Bruning, J. Mantell, R. B. Sessions, A. R. Thomson, N. R. Zaccai, R. L. Brady, P. Verkade and D. N. Woolfson, *Proc. Natl. Acad. Sci. U. S. A.*, 2012, **109**, 13266-13271.
17. P. T. Shelton and K. J. Jensen, in *Peptide Synthesis and Applications*, eds. K. J. Jensen, P. Tofteng Shelton and S. L. Pedersen, Humana Press, Totowa, NJ, 2013, ch. 2, pp. 23-41.
18. E. H. C. Bromley, K. J. Channon, P. J. S. King, Z. N. Mahmoud, E. F. Banwell, M. F. Butler, M. P. Crump, T. R. Dafforn, M. R. Hicks, J. D. Hirst, A. Rodger and D. N. Woolfson, *Biophys. J.*, 2010, **98**, 1668-1676.
19. J. Schaefer and E. O. Stejskal, *J. Am. Chem. Soc.*, 1976, **98**, 1031-1032.
20. E. Stejskal, J. Schaefer and J. Waugh, *Journal of Magnetic Resonance (1969)*, 1977, **28**, 105-112.

21. A. E. Bennett, J. H. Ok, R. G. Griffin and S. Vega, *J. Chem. Phys.*, 1992, **96**, 8624-8627.
22. A. E. Bennett, C. M. Rienstra, J. M. Griffiths, W. G. Zhen, P. T. Lansbury and R. G. Griffin, *J. Chem. Phys.*, 1998, **108**, 9463-9479.
23. K. Takegoshi, S. Nakamura and T. Terao, *Chem. Phys. Lett.*, 2001, **344**, 631-637.
24. D. Huang, B. C. Hudson, Y. Gao, E. K. Roberts and A. K. Paravastu, in *Peptide Self-Assembly: Methods and Protocols*, eds. B. L. Nilsson and T. M. Doran, Springer New York, New York, NY, 2018, ch. 2, pp. 23-68.
25. S. A. McNeill, P. L. Gor'kov, K. Shetty, W. W. Brey and J. R. Long, *J. Magn. Reson.*, 2009, **197**, 135-144.
26. M. T. Nelson, W. Humphrey, A. Gursoy, A. Dalke, L. V. Kale, R. D. Skeel and K. Schulten, *Int J Supercomput Ap*, 1996, **10**, 251-268.
27. C. W. Wood and D. N. Woolfson, *Protein Sci.*, 2018, **27**, 103-111.
28. W. Humphrey, A. Dalke and K. Schulten, *J. Mol. Graph. Model.*, 1996, **14**, 33-38.
29. J. Seo and C. Cohen, *Proteins*, 1993, **15**, 223-234.
30. K. J. Fritzsche, Y. Yang, K. Schmidt-Rohr and M. Hong, *J. Biomol. NMR*, 2013, **56**, 155-167.
31. D. S. Wishart, *Prog Nucl Mag Res Sp*, 2011, **58**, 62-87.
32. D. Wishart and B. Sykes, *J. Biomol. NMR*, 1994, **4**, 171-180.
33. S. P. Mielke and V. V. Krishnan, *J. Biomol. NMR*, 2004, **30**, 143-153.
34. S. Spera and A. Bax, *J. Am. Chem. Soc.*, 1991, **113**, 5490-5492.
35. S. G. Zech, A. J. Wand and A. E. McDermott, *J. Am. Chem. Soc.*, 2005, **127**, 8618-8626.
36. D. Huang, M. I. Zimmerman, P. K. Martin, A. J. Nix, T. L. Rosenberry and A. K. Paravastu, *J. Mol. Biol.*, 2015, **427**, 2319-2328.
37. A. Mandal, J. C. Boatz, T. B. Wheeler and P. C. van der Wel, *J. Biomol. NMR*, 2017, **67**, 165-178.
38. R. Cerpa, F. E. Cohen and I. D. Kuntz, *Fold Des.*, 1996, **1**, 91-101.
39. A. B. Siemer, C. Ritter, M. O. Steinmetz, M. Ernst, R. Riek and B. H. Meier, *J. Biomol. NMR*, 2006, **34**, 75-87.
40. M. J. Bayro, T. Maly, N. R. Birkett, C. E. Macphée, C. M. Dobson and R. G. Griffin, *Biochemistry*, 2010, **49**, 7474-7484.
41. A. K. Paravastu, A. T. Petkova and R. Tycko, *Biophys. J.*, 2006, **90**, 4618-4629.
42. B. H. Meier, R. Riek and A. Bockmann, *Trends Biochem. Sci.*, 2017, **42**, 777-787.
43. T. Watanabe-Nakayama, K. Ono, M. Itami, R. Takahashi, D. B. Teplow and M. Yamada, *Proc. Natl. Acad. Sci. U. S. A.*, 2016, **113**, 5835-5840.
44. A. T. Petkova, W. M. Yau and R. Tycko, *Biochemistry*, 2006, **45**, 498-512.
45. E. Crocker, A. B. Patel, M. Eilers, S. Jayaraman, E. Getmanova, P. J. Reeves, M. Ziliox, H. G. Khorana, M. Sheves and S. O. Smith, *J. Biomol. NMR*, 2004, **29**, 11-20.
46. M. G. Ryadnov and D. N. Woolfson, *J. Am. Chem. Soc.*, 2007, **129**, 14074-14081.
47. M. G. Ryadnov and D. N. Woolfson, *J. Am. Chem. Soc.*, 2005, **127**, 12407-12415.
48. S. V. Dvinskikh, V. Castro and D. Sandstrom, *Magn. Reson. Chem.*, 2004, **42**, 875-881.
49. V. Hronský, *Acta Electrotechnica et Informatica*, 2013, **13**.
50. A. K. Paravastu, R. D. Leapman, W. M. Yau and R. Tycko, *Proc. Natl. Acad. Sci. U. S. A.*, 2008, **105**, 18349-18354.
51. D. W. P. M. Lowik, E. H. P. Leunissen, M. van den Heuvel, M. B. Hansen and J. C. M. van Hest, *Chem. Soc. Rev.*, 2010, **39**, 3394-3412.
52. K. Chockalingam, M. Blenner and S. Banta, *Protein Eng. Des. Sel.*, 2007, **20**, 155-161.
53. J. Kopecek and J. Yang, *Angew. Chem. Int. Ed. Engl.*, 2012, **51**, 7396-7417.
54. M. J. Webber, E. A. Appel, E. W. Meijer and R. Langer, *Nature Mat.*, 2015, **15**, 13-26.
55. B. Apostolovic, M. Danial and H.-A. Klok, *Chem. Soc. Rev.*, 2010, **39**, 3541-3575.
56. R. S. Tu and M. Tirrell, *Adv. Drug Del. Rev.*, 2004, **56**, 1537-1563.
57. A. R. Cormier, C. Ruiz-Orta, R. G. Alamo and A. K. Paravastu, *Biomacromolecules*, 2012, **13**, 1794-1804.
58. A. R. Cormier, J. M. Lopez-Majada, R. G. Alamo and A. K. Paravastu, *J. Pept. Sci.*, 2013, **19**, 477-484.
59. R. A. Kammerer and M. O. Steinmetz, *J. Struct. Biol.*, 2006, **155**, 146-153.
60. H. Dong and J. D. Hartgerink, *Biomacromolecules*, 2007, **8**, 617-623.
61. B. Ciani, E. G. Hutchinson, R. B. Sessions and D. N. Woolfson, *J. Biol. Chem.*, 2002, **277**, 10150-10155.
62. M. S. de Freitas, R. Rezaei Araghi, E. Brandenburg, J. Leiterer, F. Emmerling, K. Folmert, U. I. M. Gerling-Driessen, B. Bardiaux, C. Bottcher, K. Pagel, A. Diehl, H. V. Berlepsch, H. Oschkinat and B. Koks, *J. Struct. Biol.*, 2018, **203**, 263-272.
63. T. R. Jahn, O. S. Makin, K. L. Morris, K. E. Marshall, P. Tian, P. Sikorski and L. C. Serpell, *J. Mol. Biol.*, 2010, **395**, 717-727.
64. M. O. Steinmetz, Z. Gattin, R. Verel, B. Ciani, T. Stromer, J. M. Green, P. Tittmann, C. Schulze-Bdese, H. Gross, W. F. van Gunsteren, B. H. Meier, L. C. Serpell, S. A. Mueller and R. A. Kammerer, *J. Mol. Biol.*, 2008, **376**, 898-912.
65. W. T. Astbury and H. J. Woods, *Proceedings of the Royal Society B: Biological Sciences*, 1934, **114**, 314-316.
66. B. Wang, W. Yang, J. McKittrick and M. A. Meyers, *Prog. Mater. Sci.*, 2016, **76**, 229-318.
67. D. T. Seroski, A. Restuccia, A. D. Sorrentino, K. R. Knox, S. J. Hagen and G. A. Hudalla, *Cell. Mol. Bioeng.*, 2016, **9**, 16.
68. P. J. S. King, G. M. Lizio, A. Booth, R. F. Collins, J. E. Gough, A. F. Miller and S. J. Webb, *Soft Matter*, 2016, **12**, 9.
69. J. P. Jung, A. K. Nagaraj, E. K. Fox, J. S. Rudra, J. M. Devgun and J. H. Collier, *Biomaterials*, 2009, **30**, 2400-2410.
70. A. N. Lupas and J. Bassler, *Trends Biochem. Sci.*, 2017, **42**, 130-140.



The SAF-p1/p2a binary peptide system co-assembles in water into α -helical coiled coils, but can convert post-assembly into a β -sheet structure.